RESEARCH ARTICLE OPEN ACCESS

Juvenile Myoclonic Epilepsy Imaging Endophenotypes and Relationship With Cognition and Resting-State EEG

Aaron F. Struck[1,2,3] | Camille Garcia-Ramos[1] | Klevest Gjini[1] | Jana E. Jones[1] | Vivek Prabhakaran[1,2] | Nagesh Adluru[2,4] | Bruce P. Hermann[1]

[1]Department of Neurology, University of Wisconsin School of Medicine and Public Health, Madison, Wisconsin, USA | [2]Department of Radiology, University of Wisconsin School of Medicine and Public Health, Madison, Wisconsin, USA | [3]William S Middleton Veterans Administration Hospital, Madison, Wisconsin, USA | [4]Waisman Center, University of Wisconsin-Madison, Madison, Wisconsin, USA

Correspondence: Aaron F. Struck (struck@neurology.wisc.edu)

ABSTRACT

Structural neuroimaging studies of patients with Juvenile Myoclonic Epilepsy (JME) typically present two findings: 1-volume reduction of subcortical gray matter structures, and 2-abnormalities of cortical thickness. The general trend has been to observe increased cortical thickness primarily in medial frontal regions, but heterogeneity across studies is common, including reports of decreased cortical thickness. These differences have not been explained. The cohort of patients investigated here originates from the Juvenile Myoclonic Epilepsy Connectome Project, which included comprehensive neuropsychological testing, 3 T MRI, and high-density 256-channel EEG. 64 JME patients aged 12–25 and 41 age and sex-matched healthy controls were included. Data-driven approaches were used to compare cortical thickness and subcortical volumes between the JME and control participants. After differences were identified, supervised machine learning was used to confirm their classification power. K-means clustering was used to generate imaging endophenotypes, which were then correlated with cognition, EEG frequency band lagged coherence from resting state high-density EEG, and white and grey matter based spatial statistics from diffusion imaging. The volumes of subcortical gray matter structures, particularly the thalamus and the motor-associated thalamic nuclei (ventral anterior), were found to be smaller in JME. In addition, the right hemisphere (primarily) sulcal pre-motor cortex was abnormally thicker in an age-dependent manner in JME with an asymmetry in the pre-motor cortical findings. These results suggested that for some patients JME may be an asymmetric disease, at least at the cortical level. Cluster analysis revealed three discrete imaging endophenotypes (left, right, symmetric). Clinically, the groups were not substantially different except for cognition, where left hemisphere disease was linked with a lower performance on a general cognitive factor ("g"). HD-EEG demonstrated statistically significant differences between imaging endophenotypes. Tract-based spatial statistics showed significant changes between endophenotypes as well. The left dominant disease group exhibited diffuse white matter changes. JME patients present with heterogeneity in underlying imaging endophenotypes that are defined by the presence and laterality of asymmetric abnormality at the level of the pre-motor sulcal cortex; these endophenotypes are linked to orderly relationships with cognition, EEG, and white matter pathology. The relationship of JME's adolescent onset, age-dependent cortical thickness loss, and seizure upon awakening all suggest that synaptic pruning may be a key element in the pathogenesis of JME. Individualized treatment approaches for neuromodulation are needed to target the most relevant cortical and subcortical structures as well as develop disease-modifying and neuroprotective strategies.

Summary

- Diverse data-driven methods were used to find brain anomalies in JME leading to the identification of three lateralization-based imaging endophenotypes linked to orderly relationships with cognition, EEG, and WM pathology.

- Underlying heterogeneity in JME can be harnessed to identify meaningful clinical and theoretical endophenotypes.

1 | Introduction

Juvenile Myoclonic Epilepsy (JME) is the most common generalized epilepsy in adults (Panayiotopoulos et al. 1994). JME has several distinguishing features, one being the seizure semiology. Seizures in JME are primarily motoric at onset, namely myoclonus or myoclonus evolving into a generalized tonic–clonic seizures (GTC). Despite being primarily motoric at onset, the seizures in JME are not the same as seizures originating from the primary motor cortex—where patients have repetitive clonic movements—suggesting that the seizures in JME are not originating from the primary motor cortex but likely from areas involved in motor planning.

Another interesting feature of JME is the temporality of seizures both at the onset of clinical seizures and the diurnal nature of seizures. Patients with JME typically have seizures soon after awakening. JME patients also have an onset of seizures from early adolescence until young adulthood (Canevini et al. 1992). Interestingly, adolescence and slow-wave sleep are both times of intense synaptic pruning. In adolescence, up to 50% of synaptic connections can be lost (Rakic et al. 1994) as the brain moves toward a more efficient adult pattern of activity (Chugani 1999). Similarly, in slow-wave sleep there is a rebalancing of excitation and inhibition in what is commonly termed the sleep synaptic homeostasis hypothesis (Tononi and Cirelli 2006, 2014). In this view there is a decrease of weakly connected neurons and a reinforcement of active neuronal connections consistent with a renormalization of excitation and inhibition in an activity dependent manner. The most direct evidence for this hypothesis comes from electron microscopy of mouse cortex. In mouse somatosensory cortex there is a decrease in spines of apical dendrites of layer 5 pyramidal neurons (Maret et al. 2011) following slow-wave sleep. The pressure to restore homeostasis increases with sleep-deprivation (Dijk 2009), much like the risk of seizures in JME increases following a short sleep after sleep-deprivation.

The frontal/parietal neocortex has been implicated as the site of origin for the other common generalized epilepsy—absence epilepsy. In the Genetic Absence Epilepsy rats from Strasbourg, it was found that the layer 5/6 somatosensory cortical neurons lead to epileptic spike generation (Polack et al. 2007). It would follow that JME might also have a focal onset of spikes that initiate as well in the cortex (more likely pre-motor areas) similar to this animal model of absence epilepsy. The association of JME with synaptic pruning may indicate an imbalance in local excitation and inhibition with decreased inhibitory input via asymmetric loss of GABA connections to the apical dendrites of pyramidal neurons in the pre-motor regions. The susceptibility to this process of synaptic pruning may unmask hypersynchrony leading to myoclonus with GTCs, suggesting an aberrant development of cortex and cortical–subcortical connections in the motor-associated regions. Structural imaging studies of JME have found these anticipated abnormalities, particularly with an increase in cortical thickness in the frontal regions and subcortical grey matter volume loss (Alhusaini et al. 2013; O'Muircheartaigh et al. 2011; Kim et al. 2007; Woermann et al. 1999). Indeed, one of the original findings of Janz was the presence of neuronal disorganization on autopsy (Meencke and Janz 1984)—termed microdysgenesis. Microdysgenesis is commonly referred to as mild malformations of cortical development. Typical findings are cortical laminar disorganization, abnormal cortical myelinated fibers, neuronal clustering, and heterotypic or excessively numerous neurons in white matter, subcortical areas, or cortical layers I and II (Carne 2008). Dysgenesis of cortical development is rarely a uniform process; even genetically determined diseases like tuberous sclerosis (Cohen et al. 2021), heterotopic gray matter, and genetically caused focal cortical dysplasia (Straka et al. 2022) have spatial heterogeneity.

Based on the above, we hypothesize that if JME is a disease of neurodevelopment, patients would also have asymmetrical findings on imaging that would carry clinical and cognitive implications as well as confirmatory evidence on EEG. Indeed, there are emerging reports of asymmetric seizure semiology at onset in JME (Devinsky et al. 2024; Usui et al. 2005) bolstering the case for a focal onset of this disease. We anticipate that JME would have asymmetries in cortical thickness in motor-associated areas, reduced volumes of subcortical structures involved in motor planning, and that these changes would be evident not only on imaging but also on measures of neuronal activity, namely resting state EEG. Additionally, these asymmetries should have cognitive consequences in that patients with greater involvement of the dominant hemisphere would be expected to exhibit cognitive deficits greater than expected relative to their disease severity. To address these questions, we use the cohort of patients and healthy controls from the JME Connectome Project. We examine these hypotheses by: 1-Confirming the findings of increased cortical thickness in motor-associated frontal regions and reduced volumes of subcortical gray structures, 2-Determining if any asymmetries exist in these baseline neuroimaging findings and whether they can be used to classify JME from controls, 3-Using unsupervised machine learning on imaging variables to develop endophenotypes of JME and correlate these with clinical and cognitive outcomes, and 4-Using resting state EEG and diffusion weighted imaging to determine if asymmetries using structural imaging have electrographic and/or connectivity correlates.

2 | Methods

2.1 | Participants

The participants came from the JME Connectome Project. Inclusion criteria for JME ($N = 64$) included a diagnosis of JME supported by at least two of the following: (1) clinical description or directly observed early morning myoclonic jerks, (2) clinical description or directly observed generalized tonic–clonic

seizures, (3) an EEG with bursts of 3.5–5 Hz generalized spike–wave and/or polyspike wave discharges as well as all of the following: (4) age between 12 and 25 years, (5) English speaking, (6) Verbal and Performance IQ ≥ 80. Exclusion criteria included: (1) inability to provide informed consent, (2) reported or directly observed semiological or EEG features that suggest focal epilepsy, (3) presence of any lesions other than non-specific white matter abnormalities on 3 Tesla MRI with a dedicated epilepsy protocol that includes high-resolution axial and coronal FLAIR sequences, and (4) an active infectious etiology of seizures. The control group was composed of healthy age and sex-matched JME participants from other ongoing epilepsy projects or community-based recruitment (posters and e-mail blasts). JME patients and controls were interrogated for their differential assignment to the identified latent groups.

2.2 | MRI Acquisition and Preprocessing

All JME patients underwent one 60-min 3 T MRI scanning session including high-resolution T1 and T2 structural MRI, dMRI, rs-fMRI, and ta-fMRI in the baseline visit. 3 T MRI Hardware: Scanning was done on GE MR 750 3T clinical scanners (50 mT/m & 200 T/m/s gradients) with a Nova 32-channel neuroimaging phased array receive head coil and whole-body RF transmission. MRI was performed on 3T GE 750.

Parameters for T_1-weighted images were as follows: Repetition time (TR)/echo time (TE) = 604 ms/2.516 ms, inversion time (TI) = 1060.0 ms, flip angle = 8°, field-of-view (FOV) = 25.6 cm, 0.8 mm isotropic; parameters of Cube T_2-weighted images were as follows: TR/TE = 2500 ms/94.641 ms, flip angle = 90°, FOV = 25.6 cm, 0.8 mm isotropic; and parameters of resting state functional MRI (rs-fMRI) were as follows: 8 bands, 72 slices, TR/TE = 802 ms/33.5 ms, flip angle = 50°, matrix = 104 × 104, FOV = 20.8 cm, voxel size 2 mm isotropic. Participants were asked to fixate on a white cross at the center of a black background (Glasser et al. 2013).

T_1-weighted images were B1 bias corrected using the N4 correction algorithm (Tustison et al. 2010) implemented in ANTS. These pre-processed images were then processed using the recon-all pipeline (motion correction, non-uniform intensity normalization, Talairach transform computation, intensity normalization, skull stripping, automated subcortical segmentation) in FreeSurfer (http://freesurfer.net) (version 7.4.1). The FreeSurfer script *mris_preproc* was used to compare cortical measures (i.e., thickness and volumes) between groups. It concatenates all the subjects' maps that will be used for group analyzes for each measure, hemisphere, and smoothing kernels (to improve inter-subject variability). Afterwards, *mri_glmfit* was applied to construct the model and the contrasts; it creates uncorrected contrast maps for the different measures. Then, multiple comparison cluster correction was performed using *mri_glmfit-sim* with a cluster-forming threshold set to $p = 0.05$. Group comparisons in this manuscript are all presented at a smoothing kernel of 10-mm full-width half-maximum (FWHM). Outputs for cortical thickness and cortical volumes were obtained based on both the Desikan-Killiany and the Destrieux atlases (Destrieux et al. 2010; Fischl, Salat, et al. 2004; Fischl, van der Kouwe, et al. 2004; Fischl et al. 2002); volumes of subcortical structures (e.g., thalamus, putamen, hippocampus, amygdala, caudate) were obtained from the FreeSurfer automated segmentation processing stream.

Diffusion weighted imaging data acquisition parameters were as follows. Flip angle = 90°, FOV = 21.76 cm, matrix = 128 × 128, 1.7 mm isotropic resolution, TE/TR = 76.4 ms/3361 ms, multiband factor = 4.5 $b = 0$ images, and 50 diffusion weighted images at $b = 1000 \, \text{s/mm}^2$ and $b = 2000 \, \text{s/mm}^2$ each for a total of 100 diffusion weighted images were acquired in both phase encoding (AP and PA) directions.

2.3 | Clinical and Cognitive Data

Electronic forms were used for recording demographic, medical history, neuropsychological, neurologic exam, quality of life, and electrophysiological data, based on the NIH Common Data Elements (CDE) (https://www.commondataelements.ninds.nih.gov/). These data were captured through chart review, questionnaires completed by the patient, and interviews, including a scripted interview covering details of seizure history, seizure types, and frequency. The neuropsychological test battery included measures of particular relevance in JME, most of which were drawn from the NINDS CDE for Epilepsy and selected tests from the NIH Toolbox-Cognitive Battery. Exploratory factor analysis to create a generalized cognitive factor and cognitive clusters was performed on 18 cognitive tests as described in (Struck et al. 2025).

2.4 | EEG Acquisition and Processing

High-density EEG (HD-EEG) data were acquired at a 1000 Hz sampling rate using a 256-channel system (Compumedics Neuroscan; Charlotte, North Carolina, USA) for a duration of about 45 min. The continuous EEG recording included initial awake resting state conditions (eyes open and eyes closed, of about 5-min duration each), followed by a sleep interval, and ending with an auditory oddball task of a duration of about 15 min including breaks. A clinical-grade advanced EEG signal processing and source reconstruction software (CURRY 8, Compumedics USA Inc., Charlotte, NC, USA) was used in preprocessing and display of HD-EEG data for traditional EEG reading. The EEG signals recorded were first subjected to bandpass filtering (1–70 Hz) and the application of a notch filter for line noise removal at 60 Hz. "Bad" channels were manually detected, interpolated, and then HD-EEG signals were re-referenced to the average reference. All recorded EEG traces were then visually screened by a board-certified clinical electroencephalographer in various traditional and extended montages to identify and mark the presence of epileptiform activity.

For further quantitative analyzes, HD-EEG signals were processed in EEGLAB (Delorme and Makeig 2004) a toolbox running in MATLAB (The MathWorks Inc., Natick, Massachusetts, USA). HD-EEG signals from the resting state, awake eyes closed condition were initially bandpass filtered between 1 and 100 Hz, with additional application of a notch filter at 60 Hz. Data segments heavily compromised by artifacts were detected by the EEGLAB function "clean_artifacts" and removed. The detected

"bad" channels by the same function were also removed (then later replaced by interpolated data). Physiological artifactual components (due to eye movements, muscle activity, and cardiac electric field) were detected and rejected using independent component analysis (ICA) and ICLabel (Hyvarinen 1999; Pion-Tonachini et al. 2019). After preprocessing, EEG data were low-pass filtered at 50 Hz, down sampled at 250 Hz, segmented to 3-s duration non-overlapping epochs, and further, any epochs exceeding a threshold of $\pm 100\,\mu V$ were rejected. Finally, the initial 2 min of clean signals were used for further quantitative analyzes. Lagged coherence (Pascual-Marqui 2007) was calculated using a custom Matlab script for 4 EEG bands (delta: 1–3 Hz, theta: 4–7 Hz, alpha: 8–12 Hz, and beta: 13–29 Hz), following the related formula provided in (Pascual-Marqui 2007), between all pairs of 256-ch HD-EEG signals. The application incorporates computations of spectral power density (PSD) and cross-spectral density (CSD) using non-overlapping segments of 1-s duration, as well as imaginary and real parts of coherency estimates. The connectivity matrices (256×256) were subjected to sensor-wise averaging (excluding the main diagonal values), resulting in 256 scores representing the mean connectivity for each sensor. Independent sample permutation tests ($N = 5000$ permutations), based on a t-statistic, were conducted to compare the lagged coherence estimates between groups (patients vs. controls, as well as estimates from 3 imaging clusters grouping). The threshold-free cluster enhancement (TFCE) method was used for correction for multiple comparisons (two-sided $p < 0.05$) (Mensen and Khatami 2013).

2.5 | Whole-Brain Vertex-Wise Analysis

2.5.1 | JME Versus Controls

Cortical thickness/volumes were compared between JME and unrelated healthy controls with age as a nuisance covariate using whole-brain vertex-wise analyzes, corrected for multiple comparisons using cluster correction at $p < 0.05$. These results were used to narrow the search for regions of interest (ROI) analyzes.

2.6 | Regional Cortical Thickness, Subcortical Volumes, and Thalamic Nuclei

Fifteen ROI from the motor and premotor areas were compared based on the Destrieux atlas (Supporting Information ROI S1), encompassing frontal and pericentral regions based on results from whole-brain vertex-wise analyzes. Nineteen subcortical ROI volumes were compared. Additionally, the relative volume of each thalamic nucleus to total thalamic volume was compared both with an asymmetry index and as a combined group with 50 ROIs (S1) as defined in Iglesias et al. (2018). Comparisons were performed with linear correction for age and brain volume.

2.7 | Supervised Machine Learning

Given the overall hypothesis of JME as an asymmetric disorder of neurodevelopment, particular interest was given to the relationship between reduced subcortical volumes and increased cortical thickness in pre-motor areas. A ratio was calculated for ipsilateral mean cortical thickness of the subcentral gyrus and sulcus, frontal inferior sulcus, frontal middle sulcus, frontal superior sulcus, and the ipsilateral thalamic hemisphere as in EQ1. Both regions were corrected for age and brain volume using correction for residuals. 10,000 was used as a scalar offset.

$$\text{Premotor Thalamic Ratio} = 10{,}000 * \frac{\text{Ipsilateral Mean Premotor Cortical Thickness}}{\text{Ipsilateral Thalamic Volume}} \quad (1)$$

Asymmetry indices were also calculated using Equation (2). The absolute value of the asymmetry index is used as stated in some further analysis.

$$\text{Asymmetry Index} = 100 * \frac{\text{LeftROI} - \text{RightROI}}{\text{LeftROI} + \text{RightROI}} \quad (2)$$

The asymmetry and ratio features were used in a supervised machine learning paradigm to classify JME from controls with 5-fold internal cross validation for hyperparameter tuning and external 5-fold cross validation to evaluate performance. Logistic regression, XGBOOST (Chen and Guestrin 2016), and Support Vector Machine with a radial kernel were used.

2.8 | Unsupervised Machine Learning

Imaging features were subjected to K-means clustering to identify latent imaging endophenotypes. The optimal number of clusters was determined through the stability of the Jaccard index (Jaccard 1901) (essentially that the same groups are found again with bootstrapping) and the Silhouette method (Rousseeuw 1987).

2.9 | Tract and Gray Matter Based Spatial Statistics

Preprocessing of the diffusion weighted MRI data was performed using the collection of tools implemented in FSL (Jenkinson et al. 2012), MRtrix3 (Tournier et al. 2019), and ANTS (Avants et al. 2011) following DESIGNER guidelines (Ades-Aron et al. 2018), which included the removal or mitigation of artifacts such as noise, Gibb's ringing, distortion due to eddy currents, B_1-bias, and EPI warping due to field inhomogeneities. Diffusion Tensor Imaging (DTI) parameters were estimated using the $b = 0$ and $b = 1000\,\text{s/mm}^2$ data. Neurite Orientation Dispersion and Density Imaging (NODDI) parameters were estimated using DMIPY (Fick et al. 2019).

Tract-based spatial statistics (TBSS) (Smith et al. 2007) in MNI space with TFCE and permutation testing (Smith and Nichols 2009) with 100,000 permutations was used for statistical analysis using both FA (from DTI) and neurite density (ND) and orientation dispersion index (ODI) from NODDI (Zhang et al. 2012) maps, controlling for age and sex. TBSS is a well-established and widely used voxel-wise whole-brain analysis method that helps investigate skeleton voxels within white matter tracts and identifies group-level differences in microstructural network properties. It generates statistically significant clusters, which can be anatomically labeled using a tractography atlas (Smith et al. 2007). Gray matter Based

Spatial Statistics (GBSS) (Nazeri et al. 2015, 2017) preprocessing and analysis steps were also applied using the FA and NODDI maps. Data were harmonized for slight protocol differences using neuroCombat (Fortin et al. 2017).

2.10 | Statistical Analysis

Comparison between continuous variables was performed with linear models. Comparison between categorial variables with Fisher-exact test. Group comparison of continuous variables was performed with rank-sum comparison (Wilcoxon). Significance testing was performed with two-sided p value < 0.05 with correction for multiple comparisons using false discovery rate (Benjamini 1995) from "p.adjust" base function in R. Statistical analysis of cortical and subcortical measures was performed in R (Version 4.4, R Foundation, Vienna, Austria).

3 | Results

There was no significant difference in baseline demographics for sex and age between controls and JME. On average, the patients were around 20 years old and had a duration of epilepsy of 5.9 years (Table 1).

3.1 | Group Comparison of Pre-Motor Cortex

Comparison of JME ($n=63$) and controls ($n=41$) identified an area of increased cortical volume in the right central and premotor regions (Figure S2). Region of Interest (ROI) was performed using the Destrieux atlas masked to only right frontal and central regions. Four regions (Table S2) were significant after adjustment for multiple comparisons (right subcentral gyrus and sulcus, right inferior frontal sulcus, right middle frontal sulcus and right superior frontal sulcus). A composite region composed of the mean thickness across the four pre-motor largely sulcal

TABLE 1 | Sociodemographic and clinical characteristics of participants.

	JME	Controls	p
# of subjects	63	41	
Age at imaging (years)	20.3	20.5	0.77
Sex (% female)	41 (65.0%)	22 (53.7%)	0.62
Left-handed	4 (6.3%)	1 (2.4%)	1
Age of onset (years)	14.4		
Duration (years)	5.9		
Family history epilepsy	3 (4.8%)		
Most recent GTC (months ago)	24.3		
GTC controlled by medications	78.60%		
# of ASM	1.48		

regions was then calculated for the left and right hemispheres described as "pre-motor" areas. Mean thickness for the pre-motor area on the right (2.51 mm JME, 2.45 mm controls, $p=0.010$) for the left (2.48 mm JME, 2.46 mm controls, $p=0.31$) (Figure 1A).

3.2 | Group Comparison of Subcortical Gray Matter Volume

Comparison of the 19 ROIs of subcortical gray matter volumes (S1) with linear correction for age and brain volume resulted in 16 of the 19 regions being significantly smaller in JME than in controls (Table S3). Of the subcortical structures, the thalamus had the greatest difference between JME and controls (Figure 1B).

The thalamic nuclei were compared between JME and controls as a relative proportion of the overall thalamic volume. Two motor-associated thalamic areas trended smaller in JME than in controls: the ventral anterior nucleus and the medial ventral (Reuniens) nucleus, both with $p=0.076$ after adjustment for FDR (Figure 1D and Table S4).

3.3 | Age and the Ratio of Pre-Motor Cortical Thickness to Thalamus

The hypothesis that synaptic pruning of the pre-motor cortex may play a role in JME pathogenesis was explored by examining the relationship between age and cortical thickness (Figure 2). The results show a difference in slope between controls and JME, with a significant interaction term between group membership and age on the right ($p=0.041$) and a trend on the left ($p=0.074$). Figure 2 indicates that the difference in cortical thickness is maximal at the youngest age and then reaches similar thickness by the early 20s, suggesting that this area of cortex underwent a much larger change in JME than in the controls, where a neutral to positive slope was observed (Figure 2A). In the thalamus, there was no significant interaction between group membership and age for left, $p=0.95$, and right, $p=0.29$, sides (Figure 2B). There was mostly a linear offset, where the JME patients had lower baseline volumes. These observations can be utilized to find a biologically driven measure to help differentiate JME from controls and examine focality. To this end, a ratio of the ipsilateral pre-motor cortical thickness to ipsilateral thalamic hemisphere was calculated with a 10,000 (mm^2) as normalization factor to create a unitless measure Equation (1). The right and left pre-motor to thalamic ratios between JME and controls were statistically different (Figure 1C).

Additionally, because of the reported effect of valproic acid on cortical thickness (Pimentel et al. 2023) we examined if a relationship between pre-motor cortical thickness and age differed between those patients on valproic acid ($N=10$) versus those that were not and found no significant direct or interaction effect on the left pre-motor cortex, but there was a direct effect on the right pre-motor cortex (coefficient -0.35, $p=0.047$, but non-significant interaction term $p=0.12$). There were no significant effects of valproic acid on the right (direct $p=071$, interaction $p=0.50$) or left (direct $p=0.97$, interaction $p=0.66$) thalamic volume nor in the right (direct $p=0.25$, interaction $p=0.24$) or left (direct $p=0.88$, interaction $p=0.79$) ratio of pre-motor cortical to ipsilateral thalamic volume.
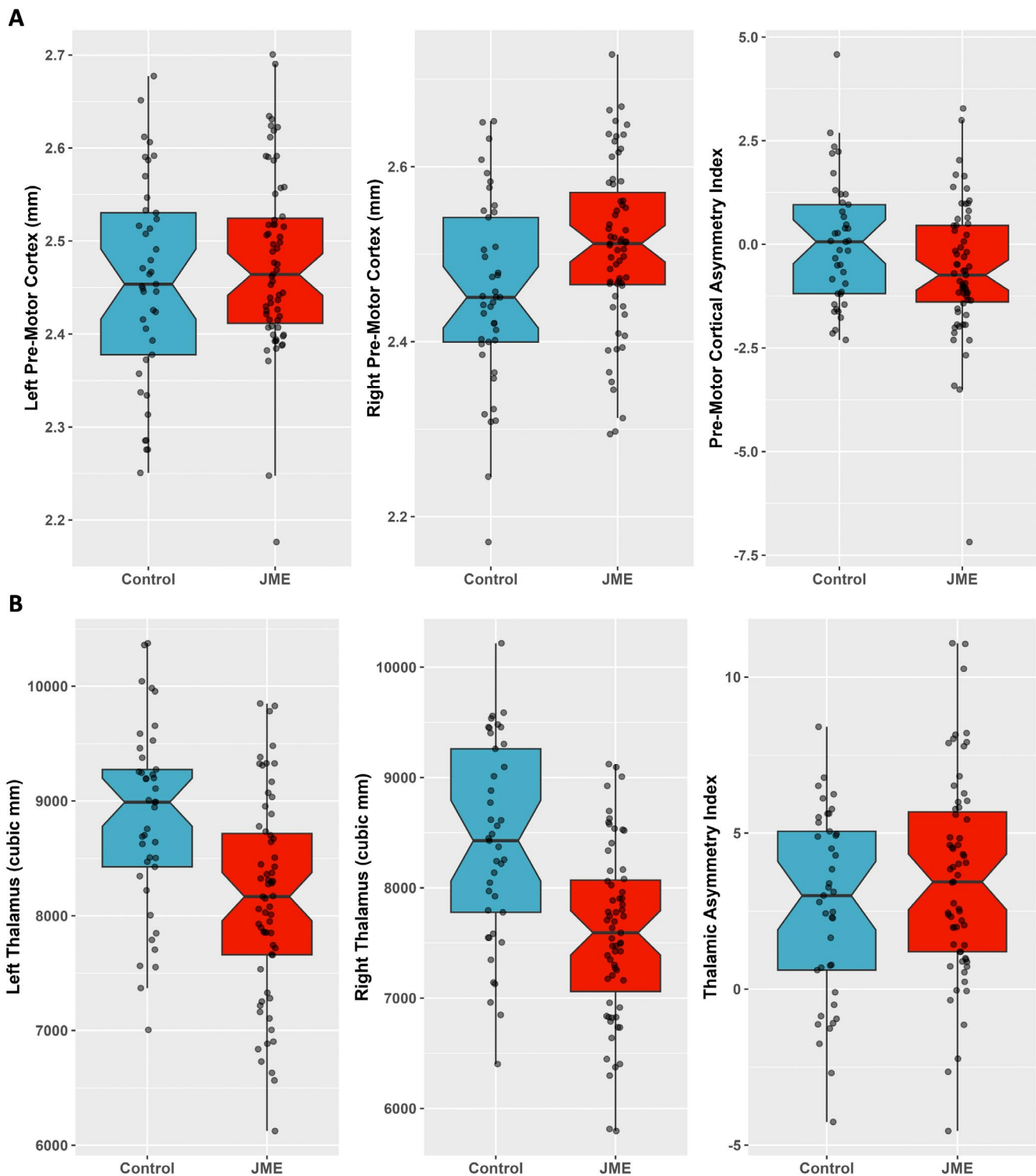
FIGURE 1 | Legend on next page.

3.4 | Asymmetry Index

Next, an asymmetry index Equation (2) was calculated for the pre-motor cortex, the thalamus, and the ratio between the two areas. There were differences in the mean asymmetry index (Figures 1A–C) for the pre-cortical regions ($p = 0.046$) and for the ratio ($p = 0.036$), but not for the thalamus ($p = 0.16$). A comparison of variance (F-statistic) was calculated on the absolute value of the asymmetry index between JME and controls with

the following results: thalamus ($p = 0.082$), pre-motor cortex ($p = 0.20$) and ratio ($p = 0.077$).

3.5 | Supervised Machine Learning

To evaluate the classification power of the imaging variables to distinguish JME from controls supervised machine learning tools were utilized. Only three variables identified in the previous
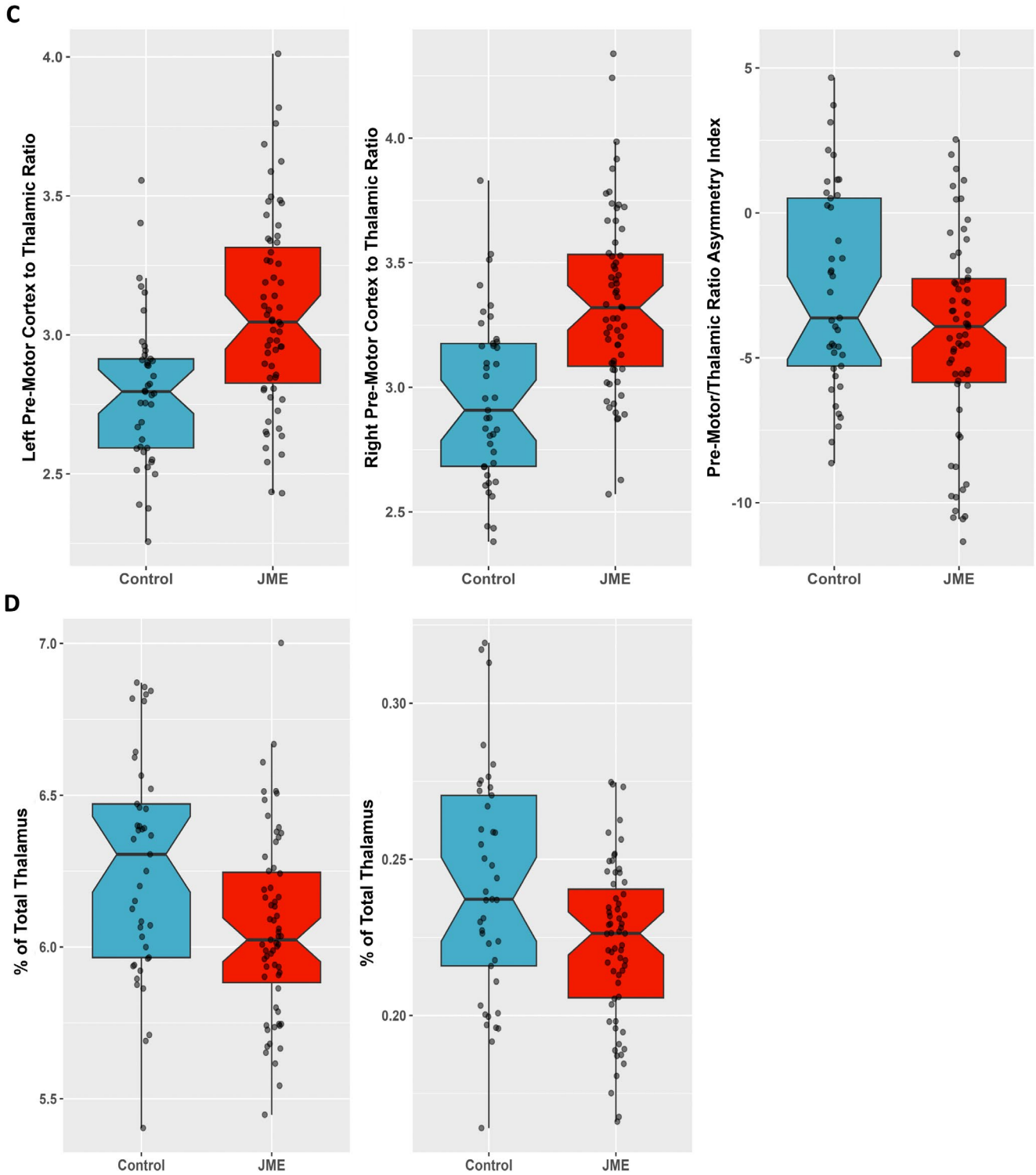
FIGURE 1 | Comparison of JME patients and healthy controls (A) for mean cortical thickness across four cortical regions corrected for age defined by the Desitreux atlas: "subcentral gyrus and sulcus", "frontal inferior frontal sulcus", "middle frontal sulcus", "superior frontal sulcus" and associated asymmetry index, (B) for thalamic volumes corrected for age and brain volume, (C) for ratio of cortex to thalamus, and (D) for thalamic nuclei as a percentage of the total nuclei. *p* values are presented with correct for FDR.

analysis were used. Several methods were employed to ensure statistical rigor and generalizability of the machine learning results. First, only three variables were used for the feature set for machine learning to avoid the "ill-poised" problem that occurs when a large number of predictive variables are used relative to the number of subjects—a so-called sparse feature set. These three variables were selected using standard statistical methods with correction for false discovery rate to prevent overfitting during feature selection. Variables included were the right and left pre-motor/thalamic ratios and the asymmetry index (Figure 1C). Next, cross-validation was utilized. In this process, 80% of the data is used to train a model, then the model is evaluated on the
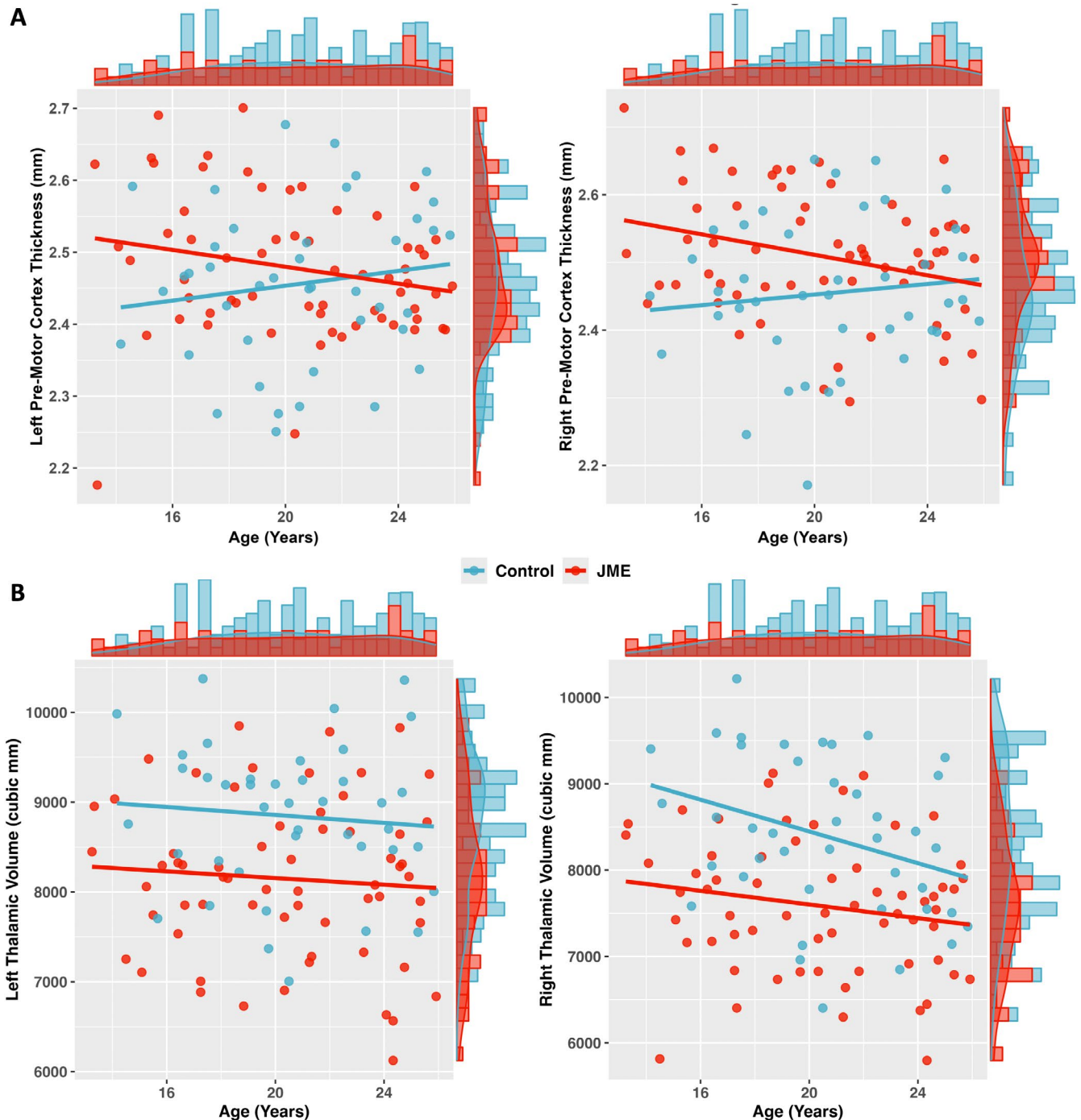
FIGURE 2 | Comparison of age versus (A) cortical thickness of the pre-motor sulcal region (B) thalamic volume (corrected for total volume) of JME and controls. Figures show significance testing for the interaction term between age and group membership: JME against controls.

remaining 20%. This process is repeated 5 times to ensure stability and hence generalizability of the results. The models were evaluated using both balanced accuracy and area under the receiver operator characteristic curve (AUC) which are standard methods of evaluating classifier performance, particularly in a balanced binary outcome measure. Next, several widely used machine learning algorithms that are suitable for relatively small datasets with few predictive variables were used, and all are present, each with similar results. XGBOOST had the best results with a mean AUC of 0.92 and balanced accuracy of 0.86. Logistic regression (AUC 0.79, Accuracy 0.73) and Support Vector Machine with linear kernel (AUC 0.79, Accuracy 0.79) had lower scores (Figure 3).

3.6 | Unsupervised Machine Learning: Imaging Endophenotypes

The previous steps identified abnormal imaging features consistent with the current understanding of JME pathophysiology, with increased pre-motor cortical thickness, particularly in the sulcal regions, and relative atrophy of the thalamus, particularly the motor thalamus. There was also greater asymmetry in these findings among patients with JME. These three variables were then shown to fairly reliably classify JME from controls using machine learning, especially using a forest-based algorithm. These results suggest that there may be underlying

endophenotypes. K-means clustering was then applied to the three variables. The optimal number of clusters was determined using the Silhouette method (Figure S5A) and confirmed with the bootstrapped (10,000 trials) Jaccard index, which was a mean of 0.81 for 2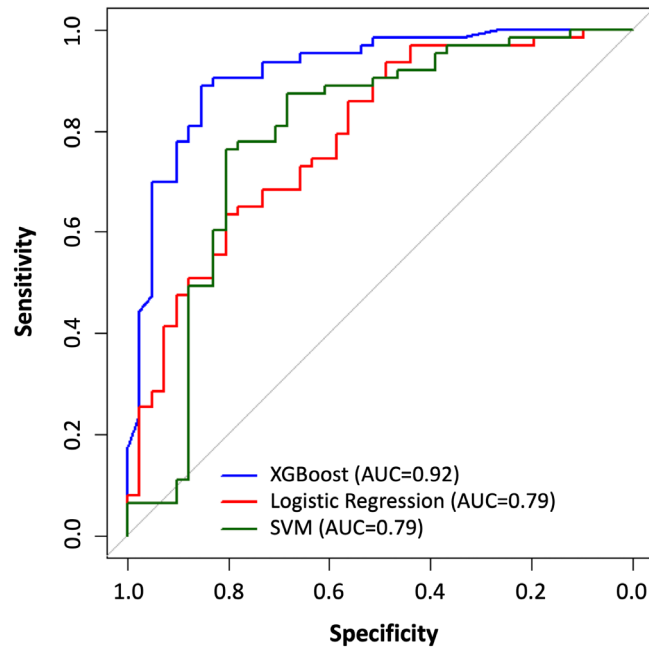 clusters, 0.94 for three clusters, and 0.83 for four clusters—demonstrating a reliable 3 cluster solution (Figure S5B). The bootstrapped Jaccard index is a process of sampling with replacement and then repeating the clustering algorithm to ensure the same clusters form repeatedly. The 3-cluster solution was reproduced 94% of the time, making it the most stable and generalizable solution. The differences in the 3 clusters are found in Figure 4 where differences between the endophenotypes were driven largely by differences in the asymmetry index (Figure 4A). The clusters were labeled based on the side with the greatest abnormality. The three clusters are termed left-lateralized ($N = 14$), symmetric ($N = 35$), and right-lateralized ($N = 14$).

FIGURE 3 | Area under the receiver operator curve (AUC) for three different machine learning algorithms applied to the classification problem of JME versus controls. Variables used in classification are the right and left cortical/thalamic ratio and the asymmetry index. 5-fold internal cross validation was used for fitting hyperparameters (e.g., cost function of SVM). External 5-fold cross-validation loops were averaged for the present AUC.

3.7 | Cognitive and Clinical Associations With Imaging Endophenotypes

Several clinical variables were evaluated between the left-lateralized, symmetric, and right-lateralized groups (Table S6). No significant differences were present. Of note, the groups are relatively small, minimizing power to detect clinical differences. Additionally, there was no statistical difference in the utilization of valproic acid between groups.

Previous work with this JME cohort led to the development of a generalized cognitive ability factor ("g") which was developed from exploratory factor analysis of a comprehensive neuropsychological test battery. This g factor is significantly different ($p < 0.0001$) between JME (mean 96.7) and controls (mean 105.3). Figure 5 shows the correlation between the left pre-motor cortical-thalamic ratio, right pre-motor cortical-thalamic ratio, and the asymmetry index. The general cognitive factor was correlated with disease severity on the left, highlighted by the significant correlation with the left ratio (Figure 5B) and the asymmetry index (Figure 5A), but not the right (Figure 5C).
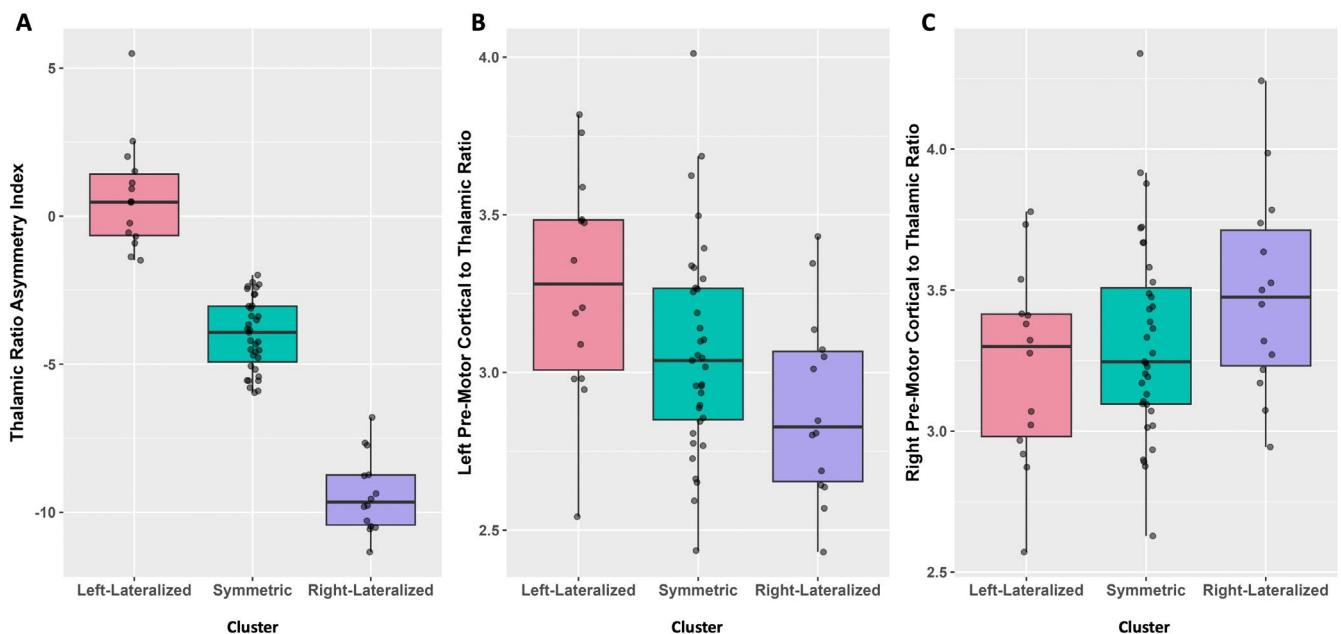

FIGURE 4 | Comparison of the underlying variables used for the unsupervised classification task that created the imaging endophenotypes: (A) Thalamic Ratio Asymmetry Index, (B) Left Pre-Motor Cortical to Thalamic Ratio, and (C) Right Pre-Motor Cortical to Thalamic Ratio.
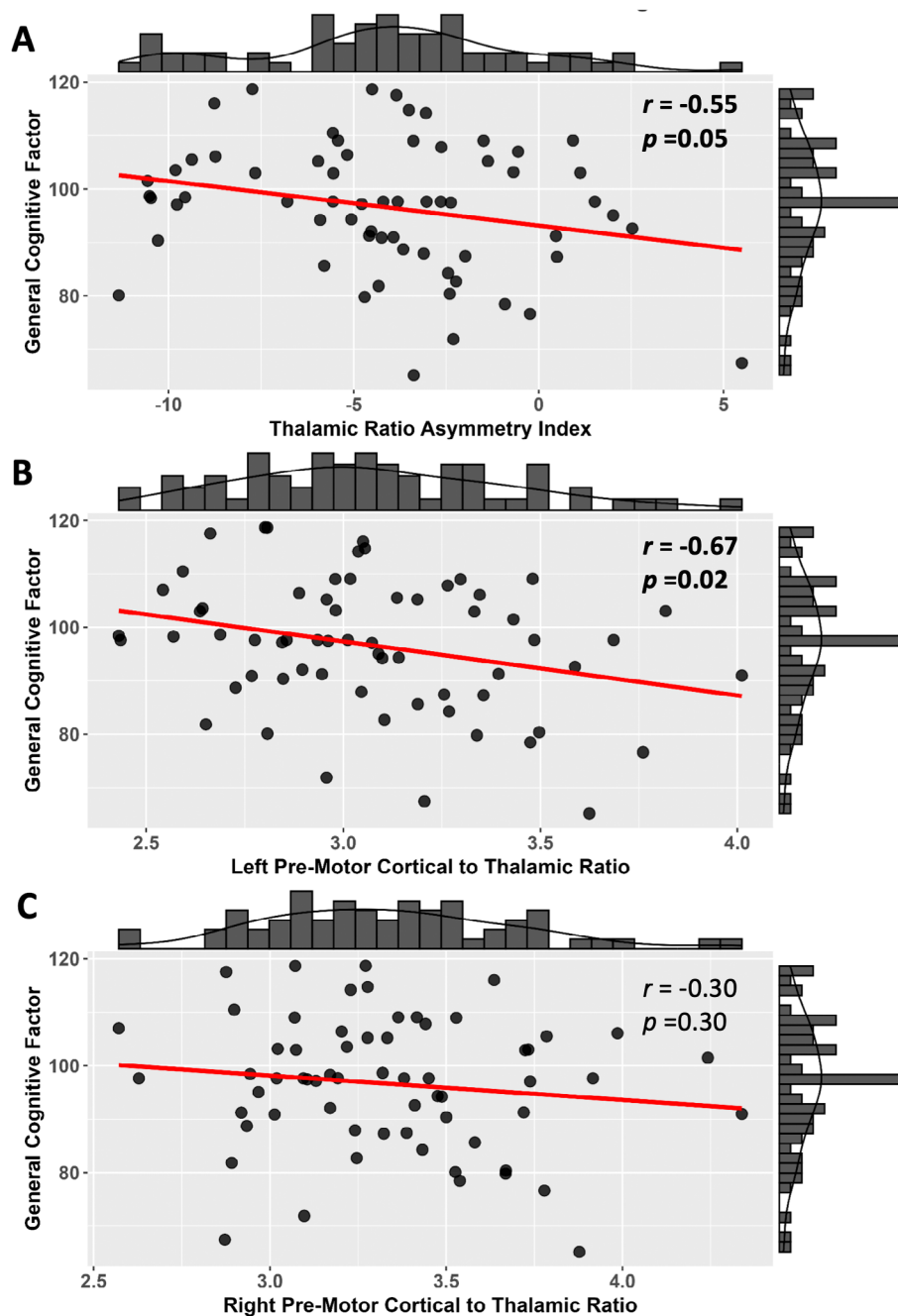
FIGURE 5 | Comparison of the three variables used to create imaging endophenotypes and a general cognitive factor: (A) Thalamic Ratio Asymmetry Index, (B) Left Pre-Motor Cortical to Thalamic Ratio, and (C) Right Pre-Motor Cortical to Thalamic Ratio.

3.8 | EEG Correlation of Imaging Endophenotypes

Most of the participants received a 256-channel high-density EEG on the day of neuroimaging and cognitive testing. Lagged coherence is a method of measuring resting state connectivity in EEG while minimizing the influence of volume conduction. Connectivity matrices were created for JME and controls for the four clinical EEG bands (delta, theta, alpha, beta). There are widespread significant differences between JME and controls in both the theta and beta bands (Figure S7). Comparison between imaging endophenotypes resulted in significant differences in the theta and beta bands between the "Left" and "Right" groups. Between the "Symmetric" and "Right" there were significant differences in the alpha and beta bands,

whereas the "Left" versus "Right" only had differences in the beta band (Figure 6). Of note, qualitative inspection across the frequency bands demonstrates a right/left asymmetry that corresponds with the underlying asymmetry from the endophenotype, particularly in the alpha and theta bands, with maybe the best example being the alpha activity in Figure 6C. The widespread differences in resting state EEG between imaging endophenotypes suggest diffuse differences in connectivity and may represent second order effects related to the structural changes likely mediated by disturbance of thalamo-cortical networks that have hemispheric impact—much like the generalized discharges of JME have a broad bilateral representation despite the more focal findings on structural imaging and the focal semiology of myoclonus. Future approaches
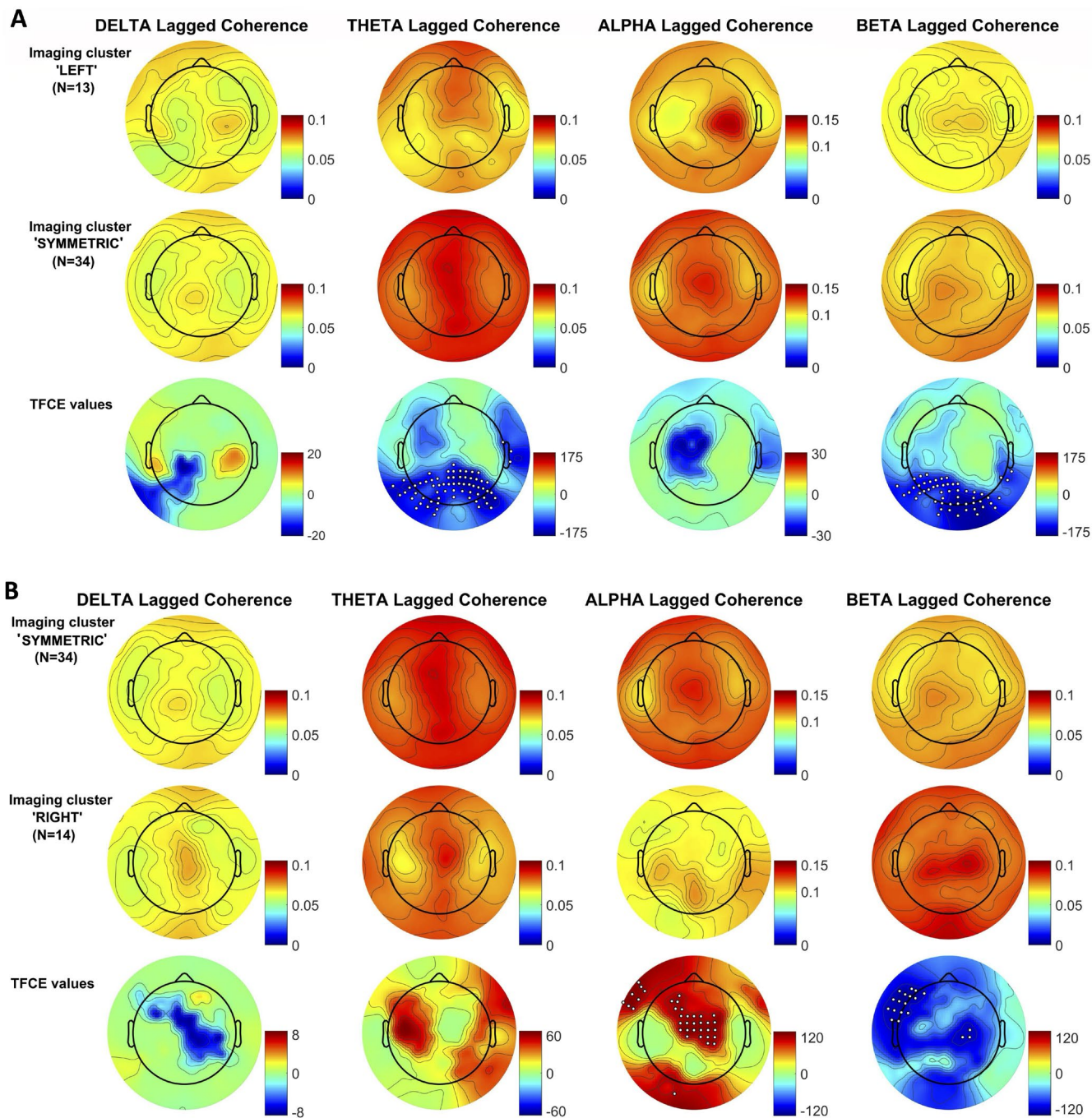
FIGURE 6 | Legend on next page.

could try and derive EEG network endophenotypes that may have a clearer correlation with cognition and seizure related variables.

3.9 | Gray Matter and TBSS Correlation With Imaging Endophenotypes

Gray matter based spatial statistics and TBSS were compared between JME and controls with no statistical differences present. Comparison of "Left", "Right", and "Symmetrical" groups demonstrated several differences. Comparison of GBSS between endophenotypes revealed minimal differences (Figure S8). Small trending widespread differences in the orientation of the

dispersion index (ODI) of the white matter tracts for the "left" group relative to "right" sided group (Figure 7B). Similarly, the "left" versus "symmetrical" group showed significant widespread differences (Figure 7A). No other differences were noted. The "left" cluster is the group that was most different from the controls. This finding suggests that the "left" endophenotype is more dispersed (less organized) relative to other JME and controls.

4 | Discussion

Here we present evidence for the following in JME: 1-an age-dependent increase in the thickness of the pre-motor sulcal
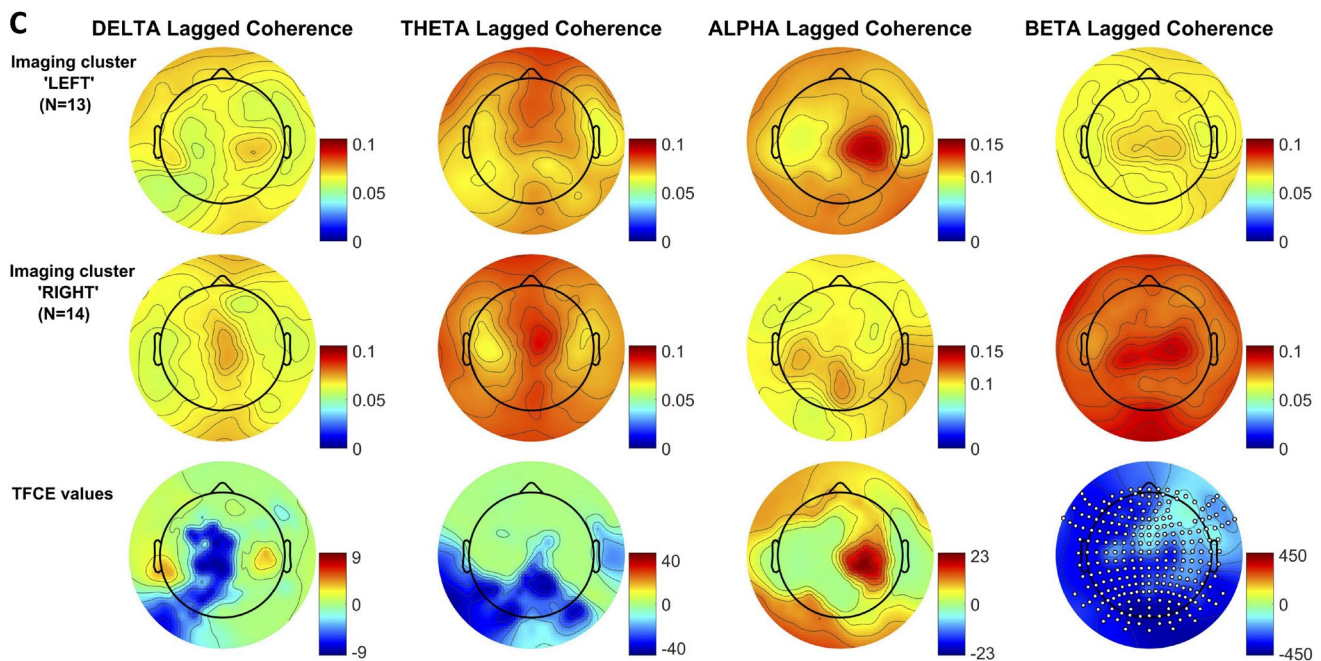
FIGURE 6 | Topoplots of mean lagged coherence for JME subjects belonging to three 'imaging clusters'—left ($N = 13$), symmetric ($N = 34$) and right ($N = 14$), as well as between group statistics (sensor-wise $p < 0.05$ corrected for multiple comparisons, highlighted with white dots): (A) Left against Symmetric, (B) Symmetric against Right, and (C) Left against Right.

cortex—this finding is more heterogeneous/asymmetric between JME patients (Figure 1A), 2-decreased volume of subcortical gray matter, particularly of the thalamus and especially the ventral anterior nucleus of the thalamus; this finding is more homogeneous among JME patients (Figure 1B), 3-heterogeneity within the structural imaging changes in JME leading to discrete imaging endophenotypes highlighting a more left, right, and symmetric imaging profile. Despite similar clinical profiles including age of onset, duration of epilepsy, and number of anti-seizure medications, it was the left-sided imaging changes that correlated most with general mental ability or "g". Resting state EEG and white matter based tract spatial statistics both provided additional neurobiological correlates of the imaging endophenotypes.

We propose a model (Figure S9) of the pathogenesis of JME based on these results and prior animal and clinical studies that start with subtle dysmorphic changes in the pre-motor cortex that are often asymmetric. These changes lead to a relative attenuation in the growth of the subcortical gray matter motor network. During adolescence, there is a synaptic pruning process that disinhibits pyramidal neurons in the pre-motor cortex, creating inelegant hypersynchronous discharges that lead to myoclonus and then sometimes quickly to bilateral tonic–clonic seizures. The nocturnal synaptic pruning recreates this disinhibition, creating seizures and myoclonus upon awakening.

4.1 | Differences in Cortical Thickness

The changes in cortical thickness related to JME have been challenging to pinpoint and vary across studies (Alhusaini et al. 2013; O'Muircheartaigh et al. 2011; Kim et al. 2007; Woermann et al. 1999). Typically, findings show increased thickness in medial frontal regions, as reported by Alhusaini et al. and Woermann et al. who identified subtle thickening

in pre-motor and frontal areas using voxel-based morphometry (Alhusaini et al. 2013; Woermann et al. 1999). However, O'Muircheartaigh et al. and Kim et al. also noted decreased thickness in some JME patients, often linking these reductions to cognitive deficits or structural abnormalities in the frontal cortex (O'Muircheartaigh et al. 2011; Kim et al. 2007), which may be influenced by medication use or neurodevelopmental processes (Pimentel et al. 2023; Lin et al. 2014). We believe these variations stem from JME not being a uniform condition, as the primary issue likely involves subtle dysmorphic changes in the sulcal regions of the frontal cortex, between the primary motor and prefrontal areas, which can differ greatly between individuals. Yet, as long as the pre-motor/thalamic/basal ganglia/cerebellar network is involved, the clinical phenotypes remain similar. This is what we observed. At the group-level, there were only minor differences in cortical thickness in the pre-motor areas, showing an age dependency consistent with Lin et al. who found cortical thickness in JME varies with age (Pimentel et al. 2023). The most significant differences appeared at the youngest ages, but as the disease progressed, cortical thickness decreased, likely due to ongoing pruning and possibly neuronal loss. This aligns with Dr. Janz's early autopsy work on JME brains, which identified microdysgenesis (Meencke and Janz 1984). The location of these imaging changes in the sulci supports this idea, as abnormalities in focal neurogenesis are more common in sulci (Macdonald-Laurs et al. 2024; Besson et al. 2008), with Besson et al. explaining the sulci's particular vulnerability (Besson et al. 2008). Large genetic studies have not found consistent monogenetic links to JME, though the best candidate genes involve ion channels (dos Santos et al. 2017). Channelopathies can cause neuronal dysgenesis, often affecting specific areas like the frontal lobe in nicotinic acetylcholine receptor epilepsy (Becchetti et al. 2015) or the temporal lobe in LGI1A-mediated autosomal dominant epilepsy with auditory features (Berkovic et al. 2004). Most
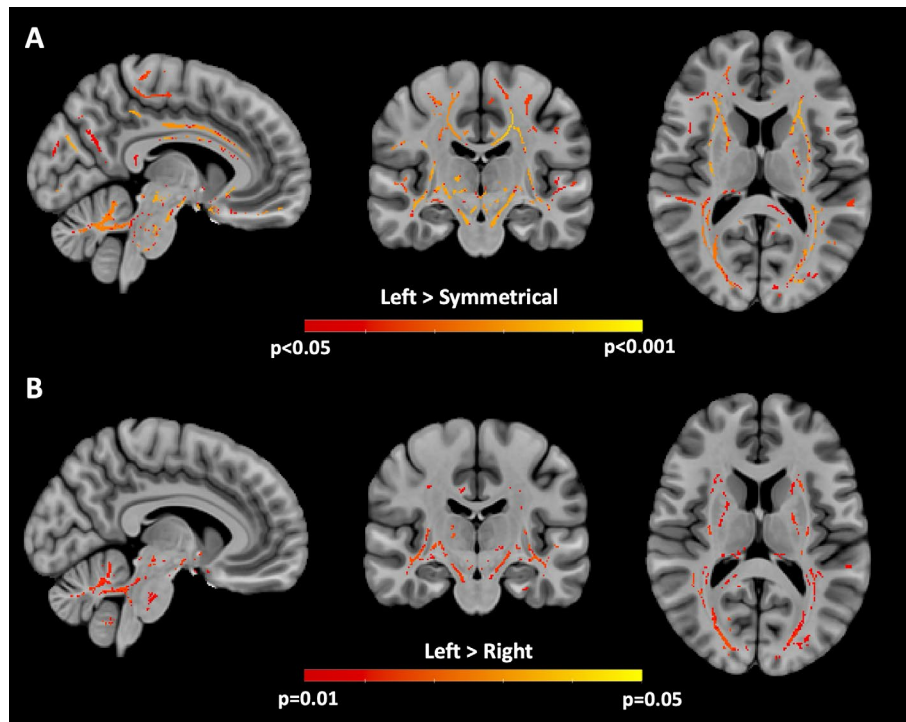
FIGURE 7 | Tract-Based Spatial Statistics (TBSS) Orientation of Dispersion Index (ODI) (A) Left Cluster ($N = 14$) > Symmetric Cluster ($N = 35$) p = red > yellow, $p < 0.10$ and > 0.05. Trending not significant corrected for age and multiple comparisons; (B) Left Cluster ($N = 14$) > Right ($N = 14$); p = red > yellow, $p < 0.05$ corrected for age and multiple comparisons, significant.

familial JME cases involve EFHC1, a microtubule-associated protein tied to radial and tangential neuronal migration (Suzuki et al. 2004; Annesi et al. 2007; de Nijs et al. 2012). The discrepancies in JME structural imaging studies of cortical thickness may arise from individual-level heterogeneity in subtle pre-motor sulcal microdysgenesis, further complicated by age-related synaptic pruning. Still, the subcortical networks in JME should be more consistent across patients.

4.2 | Subcortical Differences

The subcortical imaging changes did not have the asymmetry of the cortical changes. It was relatively uniform that JME patients had decreased volumes of the subcortical gray matter and cerebellum, particularly of the thalamus and especially the ventral anterior nucleus of the thalamus. It was a common pathway among JME to have relative atrophy of the motor thalamus, cerebellum, and basal ganglion. Dysfunction of this pre-motor network may give rise to the myoclonus of JME. Once the disinhibition of the pyramidal layer 5/6 neurons of the pre-motor cortex occurs from synaptic pruning, the area loses the precision feedback from interneurons, resulting in hypersynchronous discharges with rapid synchronization across the corpus callosum, leading to myoclonus that can quickly spread to a bilateral tonic clonic seizure.

4.3 | Endophenotypes and Correlation With Disease Characteristics and Cognition

Based only on the three measures of pre-motor cortical to thalamus ratio on the right, left, and the asymmetry index, there was

reasonable (AUC > 0.9) classification power of JME from controls. Those three measures also reliably clustered into three groups we termed "endophenotypes". Those endophenotypes were differentiated by how lateralized the imaging changes were. The three groups did not differentiate in any meaningful way clinically other than one—similar in terms of age of onset, gender distribution, epilepsy duration, number of medications, and seizure frequency—but not cognition. There was no direct group difference in the general cognitive factor "g" however, these are relatively small groups. With a correlation analysis between the three measures used to create the endophenotypes and "g", a clear pattern emerged. The asymmetry index and the left-sided cortical-thalamic ratio were both significant predictors of "g" while the right was not. Essentially, the more left-sided the disease, the greater the cognitive deficit. So, while the clinical syndrome itself did not see much difference between endophenotypes (as would be expected with a well-established clinical syndrome like JME), there was an impact in cognition, and it is logical that the more left-sided or dominant hemisphere the disease, the more deficit would be expected in the general cognitive factor. So, more important for the cognitive impact of JME is whether the disease is more right- or left-sided than if the seizures are well controlled. There were no other meaningful clinical differences between these groups, suggesting the left pre-motor network may play an important role in executive functioning critical to supporting general cognition, but further examination of this hypothesis is needed.

4.4 | EEG Association

There were abnormalities in resting state EEG connectivity of epilepsy patients at baseline (Elkholy 2023; Issabekov

et al. 2024; Xu et al. 2021; Shakeshaft et al. 2022), a finding that is probably underused for diagnosis and localization in clinical epilepsy. Here we examined whether the differences in theta and beta band connectivity that are present between JME and controls might also reflect the differences between the imaging endophenotypes. They did, as there were significant differences in that the beta band lagged coherence between all the groups. Theta activity was significant in the left versus symmetric, and alpha activity was significantly different between the symmetric versus right. The peak band coherence also reflected the asymmetry in the imaging endophenotypes for the theta and alpha activity, though it did not reach statistical significance in all cases, but Figure 6C (right versus left) highlights this qualitative finding the most.

4.5 | Diffusion Based Measures

Interestingly, there were minimal differences detectable using GBSS between JME and controls or within JME endophenotypes. Again, these findings speak to the heterogeneity in the cortical changes within JME. The white matter based spatial statistics also did not reveal any significant results between JME and controls. However, the endophenotypes had a difference in that the "left" group had widespread trending differences compared to the "right" and significant differences compared to the "symmetric" group. The "left" had widespread increased ODI. The right and symmetric groups had minimal differences. This "left" group was the most different from controls, whereas the right and symmetric group was more similar to controls. It is also this "left" group that has the lowest general cognitive factor. It shows potentially how subtle "left" cortical changes in critical areas can lead to widespread changes in white matter tracts that influence the general cognitive factors. The increased ODI in the left group would suggest a less organized white matter bundles in the "left" sided JME group.

4.6 | Limitations and Future Directions

There are numerous limitations to this dataset and a need for further study. The proposed cortical abnormalities are quite subtle and heterogeneous. Improved hardware techniques include high-gradient, high-performance scanners like MAGNUS (Foo et al. 2020) or high-magnetmagnet-strength scanners that are needed to confirm these changes. Additionally, flexible statistical/ML methods are needed to account for variability within JME.

Statistical techniques such as threshold-free network-based statistics (TFNBS) (Chu et al. 2023; Baggio et al. 2018) and topological data analysis methods (Phillips et al. 2024; Sizemore et al. 2019) and fixel based analysis (FBA) (Mito et al. 2024) that look for individual-level differences are required. With these advances, more personalized treatment approaches can be achieved. Additional microstructural measures such as those from Diffusion Kurtosis Imaging (DKI) (Fieremans et al. 2011; Kang et al. 2021), White Matter Tract Integrity Measures (WMTI) (Fieremans et al. 2013), and Standard Model Imaging (SMI) (Coelho et al. 2022; Novikov et al. 2019) can be derived from diffusion weighted MRI data. These models can offer complementary information to those of NODDI measures and can shed light on the microstructural alterations due to JME (Goodman and Szaflarski 2021).

To examine the synaptic pruning hypothesis, several steps are required, including longitudinal structural/connectivity imaging, pre-and post-sleep molecular imaging, or other techniques like TMS-EEG to gauge the effect of sleep on connectivity/synaptic density. The effects of genetics, epigenetics, and socioeconomic environment as they relate to the process of abnormal cortical development that leads to JME and related disorders need further study, including the use of polygenic risk scores and area deprivation index. There may be methods to prevent the manifestations of JME in at-risk individuals.

Ultimately, our goal is to identify the patient-specific mechanism leading to seizures, affective, and/or cognitive dysfunction in patients with JME in order to provide targeted therapeutics. In this case, we demonstrate that neuromodulatory strategies may need to be individualized if targeting cortical structures. If the disease process is predominately lateralized or the network disturbance is limited to pre-motor regions, targeted non-invasive neuromodulation is possible with direct current, alternating current, or even with emerging technologies like low-intensity focused ultrasound. Or, if subcortical structures are targeted with tools like beep brain stimulation or responsive neurostimulation, traditional targets like the centromedian, pulvinar, and anterior nucleus are not the optimal targets—ventral anterior or cerebellar nuclei could be considered. Refined diagnostics and classification of JME in particular and idiopathic generalized epilepsy generally using quantitative neuroimaging and/or EEG methods (and potentially genetic) may become necessary as clinical presentation and spike biomarkers may not be sufficient to improve therapeutic approaches. We also found that the cognitive deficits associated with JME were not just correlated with typical markers of disease severity like the number of seizures. In fact, it was the structural and white matter changes that better predicted cognitive status. To treat the epilepsy patient fully will also require addressing these concerns. This study is but one of the growing pieces of evidence of focality within generalized epilepsy and draws into question whether the pragmatic clinical distinction of focal versus generalized epilepsy is in fact a broken dichotomy and needs to be replaced with the concept of epilepsy as a network disease (Scharfman et al. 2018).

Ethics Statement

We confirm that we have read the Journal's position on issues involved in ethical publication and affirm that this report is consistent with those guidelines.

Conflicts of Interest

The authors declare no conflicts of interest.

Data Availability Statement

Datasets analyzed in this study are not publicly available, but further information about the datasets is available from the corresponding author on reasonable request.

References

Ades-Aron, B., J. Veraart, P. Kochunov, et al. 2018. "Evaluation of the Accuracy and Precision of the Diffusion Parameter EStImation With Gibbs and NoisE Removal Pipeline." *NeuroImage* 183: 532–543. https://doi.org/10.1016/j.neuroimage.2018.07.066.

Alhusaini, S., L. Ronan, C. Scanlon, et al. 2013. "Regional Increase of Cerebral Cortex Thickness in Juvenile Myoclonic Epilepsy." *Epilepsia* 54, no. 9: e138–e141. https://doi.org/10.1111/epi.12330.

Annesi, F., A. Gambardella, R. Michelucci, et al. 2007. "Mutational Analysis of EFHC1 Gene in Italian Families With Juvenile Myoclonic Epilepsy." *Epilepsia* 48, no. 9: 1686–1690. https://doi.org/10.1111/j.1528-1167.2007.01173.x.

Avants, B. B., N. J. Tustison, G. Song, P. A. Cook, A. Klein, and J. C. Gee. 2011. "A Reproducible Evaluation of ANTs Similarity Metric Performance in Brain Image Registration." *NeuroImage* 54, no. 3: 2033–2044. https://doi.org/10.1016/j.neuroimage.2010.09.025.

Baggio, H. C., A. Abos, B. Segura, et al. 2018. "Statistical Inference in Brain Graphs Using Threshold-Free Network-Based Statistics." *Human Brain Mapping* 39, no. 6: 2289–2302. https://doi.org/10.1002/hbm.24007.

Becchetti, A., P. Aracri, S. Meneghini, S. Brusco, and A. Amadeo. 2015. "The Role of Nicotinic Acetylcholine Receptors in Autosomal Dominant Nocturnal Frontal Lobe Epilepsy." *Frontiers in Physiology* 6: 22. https://doi.org/10.3389/fphys.2015.00022.

Benjamini, Y. H. W. 1995. "Controlling the False Discovery Rate: A Practical and Powerful Approach to Multiple Testing." *Journal of the Royal Statistical Soceity* 57, no. 1: 289–300.

Berkovic, S. F., P. Izzillo, J. M. McMahon, et al. 2004. "LGI1 Mutations in Temporal Lobe Epilepsies." *Neurology* 62, no. 7: 1115–1119. https://doi.org/10.1212/01.WNL.0000118213.94650.81.

Besson, P., F. Andermann, F. Dubeau, and A. Bernasconi. 2008. "Small Focal Cortical Dysplasia Lesions Are Located at the Bottom of a Deep Sulcus." *Brain* 131, no. 12: 3246–3255. https://doi.org/10.1093/brain/awn224.

Canevini, M. P., R. Mai, C. Di Marco, et al. 1992. "Juvenile Myoclonic Epilepsy of Janz: Clinical Observations in 60 Patients." *Seizure* 1, no. 4: 291–298. https://doi.org/10.1016/1059-1311(92)90039-4.

Carne, R. 2008. "Neurology and Clinical Neuroscience–By AHV Schapira." *Internal Medicine Journal* 38, no. 12: 932–933. https://doi.org/10.1111/j.1445-5994.2008.01838.x.

Chen, T., and C. Guestrin. 2016. "XGBoost: A Scalable Tree Boosting System." In Proceedings of the 22nd ACM SIGKDD International Conference on Knowledge Discovery and Data Mining: KDD '16, 785–794. Association for Computing Machinery.

Chu, D. Y., N. Adluru, V. A. Nair, et al. 2023. "Association of Neighborhood Deprivation With White Matter Connectome Abnormalities in Temporal Lobe Epilepsy." *Epilepsia* 64, no. 9: 2484–2498. https://doi.org/10.1111/epi.17702.

Chugani, H. T. 1999. "Review: Metabolic Imaging: A Window on Brain Development and Plasticity." *Neuroscientist* 5, no. 1: 29–40. https://doi.org/10.1177/107385849900500105.

Coelho, S., S. H. Baete, G. Lemberskiy, et al. 2022. "Reproducibility of the Standard Model of Diffusion in White Matter on Clinical MRI Systems." *NeuroImage* 257: 119290. https://doi.org/10.1016/j.neuroimage.2022.119290.

Cohen, A. L., B. P. Mulder, A. K. Prohl, et al. 2021. "Tuber Locations Associated With Infantile Spasms Map to a Common Brain Network." *Annals of Neurology* 89, no. 4: 726–739. https://doi.org/10.1002/ana.26015.

de Nijs, L., N. Wolkoff, B. Coumans, A. V. Delgado-Escueta, T. Grisar, and B. Lakaye. 2012. "Mutations of EFHC1, Linked to Juvenile Myoclonic Epilepsy, Disrupt Radial and Tangential Migrations During Brain Development." *Human Molecular Genetics* 21, no. 23: 5106–5117. https://doi.org/10.1093/hmg/dds356.

Delorme, A., and S. Makeig. 2004. "EEGLAB: An Open Source Toolbox for Analysis of Single-Trial EEG Dynamics Including Independent Component Analysis." *Journal of Neuroscience Methods* 134, no. 1: 9–21. https://doi.org/10.1016/j.jneumeth.2003.10.009.

Destrieux, C., B. Fischl, A. Dale, and E. Halgren. 2010. "Automatic Parcellation of Human Cortical Gyri and Sulci Using Standard Anatomical Nomenclature." *NeuroImage* 53, no. 1: 1–15. https://doi.org/10.1016/j.neuroimage.2010.06.010.

Devinsky, O., C. Elder, S. Sivathamboo, I. E. Scheffer, and M. J. Koepp. 2024. "Idiopathic Generalized Epilepsy: Misunderstandings, Challenges, and Opportunities." *Neurology* 102, no. 3: e208076. https://doi.org/10.1212/WNL.0000000000208076.

Dijk, D. J. 2009. "Regulation and Functional Correlates of Slow Wave Sleep." *Journal of Clinical Sleep Medicine* 5, no. 2 Suppl: S6–S15.

dos Santos, B. P., C. R. M. Marinho, and T. E. B. S. Marques. 2017. "Genetic Susceptibility in Juvenile Myoclonic Epilepsy: Systematic Review of Genetic Association Studies." *PLoS One* 12, no. 6: e0179629. https://doi.org/10.1371/journal.pone.0179629.

Elkholy, M. M. 2023. "Disruption of EEG Resting State Functional Connectivity in Patients With Focal Epilepsy." *Egyptian Journal of Neurology, Psychiatry and Neurosurgery* 59, no. 1: 122. https://doi.org/10.1186/s41983-023-00727-2.

Fick, R. H. J., D. Wassermann, and R. Deriche. 2019. "The Dmipy Toolbox: Diffusion MRI Multi-Compartment Modeling and Microstructure Recovery Made Easy." *Frontiers in Neuroinformatics* 13: 64. https://doi.org/10.3389/fninf.2019.00064.

Fieremans, E., A. Benitez, J. H. Jensen, et al. 2013. "Novel White Matter Tract Integrity Metrics Sensitive to Alzheimer Disease Progression." *American Journal of Neuroradiology* 34, no. 11: 2105–2112. https://doi.org/10.3174/ajnr.A3553.

Fieremans, E., J. H. Jensen, and J. A. Helpern. 2011. "White Matter Characterization With Diffusional Kurtosis Imaging." *NeuroImage* 58, no. 1: 177–188. https://doi.org/10.1016/j.neuroimage.2011.06.006.

Fischl, B., A. van der Kouwe, C. Destrieux, et al. 2004. "Automatically Parcellating the Human Cerebral Cortex." *Cerebral Cortex* 14, no. 1: 11–22.

Fischl, B., D. H. Salat, A. J. van der Kouwe, et al. 2004. "Sequence-Independent Segmentation of Magnetic Resonance Images." *NeuroImage* 23, no. Suppl 1: S69–S84. https://doi.org/10.1016/j.neuroimage.2004.07.016.

Fischl, B., D. H. Salat, E. Busa, et al. 2002. "Whole Brain Segmentation: Automated Labeling of Neuroanatomical Structures in the Human Brain." *Neuron* 33, no. 3: 341–355.

Foo, T. K. F., E. T. Tan, M. E. Vermilyea, et al. 2020. "Highly Efficient Head-Only Magnetic Field Insert Gradient Coil for Achieving Simultaneous High Gradient Amplitude and Slew Rate at 3.0T (MAGNUS) for Brain Microstructure Imaging." *Magnetic Resonance in Medicine* 83, no. 6: 2356–2369. https://doi.org/10.1002/mrm.28087.

Fortin, J. P., D. Parker, B. Tunç, et al. 2017. "Harmonization of Multi-Site Diffusion Tensor Imaging Data." *NeuroImage* 161: 149–170. https://doi.org/10.1016/j.neuroimage.2017.08.047.

Glasser, M., S. N. Sotiropoulos, J. A. Wilson, et al. 2013. "The Minimal Preprocessing Pipelines for the Human Connectome Project." *NeuroImage* 80: 105–124. https://doi.org/10.1016/j.neuroimage.2013.04.127.

Goodman, A. M., and J. P. Szaflarski. 2021. "Recent Advances in Neuroimaging of Epilepsy." *Neurotherapeutics* 18, no. 2: 811–826. https://doi.org/10.1007/s13311-021-01049-y.

Hyvarinen, A. 1999. "Fast and Robust Fixed-Point Algorithms for Independent Component Analysis." *IEEE Transactions on Neural Networks* 10, no. 3: 626–634. https://doi.org/10.1109/72.761722.

Iglesias, J. E., R. Insausti, G. Lerma-Usabiaga, et al. 2018. "A Probabilistic Atlas of the Human Thalamic Nuclei Combining Ex Vivo MRI and Histology." https://doi.org/10.48550/arXiv.1806.08634.

Issabekov, G., T. Matsumoto, H. Hoshi, K. Fukasawa, S. Ichikawa, and Y. Shigihara. 2024. "Resting-State Brain Activity Distinguishes Patients With Generalised Epilepsy From Others." *Seizure: European Journal of Epilepsy* 115: 50–58. https://doi.org/10.1016/j.seizure.2024.01.001.

Jaccard, P. 1901. "Étude Comparative de la Distribution Florale Dans Une Portion Des Alpes et du Jura." *Bulletin de la Société Vaudoise Des Sciences Naturelles* 37, no. 142: 547. https://doi.org/10.5169/seals-266450.

Jenkinson, M., C. F. Beckmann, T. E. J. Behrens, M. W. Woolrich, and S. M. Smith. 2012. "FSL." *NeuroImage* 62, no. 2: 782–790. https://doi.org/10.1016/j.neuroimage.2011.09.015.

Kang, L., J. Chen, J. Huang, T. Zhang, and J. Xu. 2021. "Identifying Epilepsy Based on Machine-Learning Technique With Diffusion Kurtosis Tensor." *CNS Neuroscience & Therapeutics* 28, no. 3: 354–363. https://doi.org/10.1111/cns.13773.

Kim, J. H., J. K. Lee, S. B. Koh, et al. 2007. "Regional Grey Matter Abnormalities in Juvenile Myoclonic Epilepsy: A Voxel-Based Morphometry Study." *NeuroImage* 37, no. 4: 1132–1137. https://doi.org/10.1016/j.neuroimage.2007.06.025.

Lin, J. J., K. Dabbs, J. D. Riley, et al. 2014. "Neurodevelopment in New-Onset Juvenile Myoclonic Epilepsy Over the First 2 Years." *Annals of Neurology* 76, no. 5: 660–668. https://doi.org/10.1002/ana.24240.

Macdonald-Laurs, E., A. E. L. Warren, P. Francis, et al. 2024. "The Clinical, Imaging, Pathological and Genetic Landscape of Bottom-Of-Sulcus Dysplasia." *Brain* 147, no. 4: 1264–1277. https://doi.org/10.1093/brain/awad379.

Maret, S., U. Faraguna, A. B. Nelson, C. Cirelli, and G. Tononi. 2011. "Sleep and Wake Modulate Spine Turnover in the Adolescent Mouse Cortex." *Nature Neuroscience* 14, no. 11: 1418–1420. https://doi.org/10.1038/nn.2934.

Meencke, H. J., and D. Janz. 1984. "Neuropathological Findings in Primary Generalized Epilepsy: A Study of Eight Cases." *Epilepsia* 25, no. 1: 8–21. https://doi.org/10.1111/j.1528-1157.1984.tb04149.x.

Mensen, A., and R. Khatami. 2013. "Advanced EEG Analysis Using Threshold-Free Cluster-Enhancement and Non-Parametric Statistics." *NeuroImage* 67: 111–118. https://doi.org/10.1016/j.neuroimage.2012.10.027.

Mito, R., M. Pedersen, H. Pardoe, et al. 2024. "Exploring Individual Fixel-Based White Matter Abnormalities in Epilepsy." *Brain Communications* 6, no. 1: fcad352. https://doi.org/10.1093/braincomms/fcad352.

Nazeri, A., B. H. Mulsant, T. K. Rajji, et al. 2017. "Gray Matter Neuritic Microstructure Deficits in Schizophrenia and Bipolar Disorder." *Biological Psychiatry* 82, no. 10: 726–736. https://doi.org/10.1016/j.biopsych.2016.12.005.

Nazeri, A., M. M. Chakravarty, and D. J. Rotenberg. 2015. "Functional Consequences of Neurite Orientation Dispersion and Density in Humans Across the Adult Lifespan." *Journal of Neuroscience* 35, no. 4: 1753–1762. https://doi.org/10.1523/JNEUROSCI.3979-14.2015.

Novikov, D. S., E. Fieremans, S. N. Jespersen, and V. G. Kiselev. 2019. "Quantifying Brain Microstructure With Diffusion MRI: Theory and Parameter Estimation." *NMR in Biomedicine* 32, no. 4: e3998. https://doi.org/10.1002/nbm.3998.

O'Muircheartaigh, J., C. Vollmar, G. J. Barker, et al. 2011. "Focal Structural Changes and Cognitive Dysfunction in Juvenile Myoclonic Epilepsy." *Neurology* 76, no. 1: 34–40. https://doi.org/10.1212/WNL.0b013e318203e93d.

Panayiotopoulos, C. P., T. Obeid, and A. R. Tahan. 1994. "Juvenile Myoclonic Epilepsy: A 5-Year Prospective Study." *Epilepsia* 35, no. 2: 285–296. https://doi.org/10.1111/j.1528-1157.1994.tb02432.x.

Pascual-Marqui, R. D. 2007. "Discrete, 3D Distributed, Linear Imaging Methods of Electric Neuronal Activity. Part 1: Exact, Zero Error Localization." https://doi.org/10.48550/arXiv.0710.3341.

Phillips, J. S., N. Adluru, M. K. Chung, et al. 2024. "Greater White Matter Degeneration and Lower Structural Connectivity in Non-Amnestic vs. Amnestic Alzheimer's Disease." *Frontiers in Neuroscience* 18: 1353306. https://doi.org/10.3389/fnins.2024.1353306.

Pimentel, B. C., G. Kuchukhidze, F. Xiao, et al. 2023. "Imaging Drug Resistance in Juvenile Myoclonic Epilepsy With MRI-Derived Cortical Markers." https://doi.org/10.1101/2023.12.03.23298783.

Pion-Tonachini, L., K. Kreutz-Delgado, and S. Makeig. 2019. "ICLabel: An Automated Electroencephalographic Independent Component Classifier, Dataset, and Website." *NeuroImage* 198: 181–197. https://doi.org/10.1016/j.neuroimage.2019.05.026.

Polack, P. O., I. Guillemain, E. Hu, C. Deransart, A. Depaulis, and S. Charpier. 2007. "Deep Layer Somatosensory Cortical Neurons Initiate Spike-And-Wave Discharges in a Genetic Model of Absence Seizures." *Journal of Neuroscience* 27, no. 24: 6590–6599. https://doi.org/10.1523/JNEUROSCI.0753-07.2007.

Rakic, P., J. P. Bourgeois, and P. S. Goldman-Rakic. 1994. "Synaptic Development of the Cerebral Cortex: Implications for Learning, Memory, and Mental Illness." *Progress in Brain Research* 102: 227–243. https://doi.org/10.1016/S0079-6123(08)60543-9.

Rousseeuw, P. J. 1987. "Silhouettes: A Graphical Aid to the Interpretation and Validation of Cluster Analysis." *Journal of Computational and Applied Mathematics* 20: 53–65. https://doi.org/10.1016/0377-0427(87)90125-7.

Scharfman, H. E., A. M. Kanner, A. Friedman, et al. 2018. "Epilepsy as a Network Disorder (2): What Can We Learn From Other Network Disorders Such as Dementia and Schizophrenia, and What Are the Implications for Translational Research?" *Epilepsy & Behavior* 78: 302–312. https://doi.org/10.1016/j.yebeh.2017.09.016.

Shakeshaft, A., P. Laiou, E. Abela, et al. 2022. "Heterogeneity of Resting-State EEG Features in Juvenile Myoclonic Epilepsy and Controls." *Brain Communications* 4, no. 4: fcac180. https://doi.org/10.1093/braincomms/fcac180.

Sizemore, A. E., J. E. Phillips-Cremins, R. Ghrist, and D. S. Bassett. 2019. "The Importance of the Whole: Topological Data Analysis for the Network Neuroscientist." *Network Neuroscience* 3, no. 3: 656–673. https://doi.org/10.1162/netn_a_00073.

Smith, S. M., and T. E. Nichols. 2009. "Threshold-Free Cluster Enhancement: Addressing Problems of Smoothing, Threshold Dependence and Localisation in Cluster Inference." *NeuroImage* 44, no. 1: 83–98. https://doi.org/10.1016/j.neuroimage.2008.03.061.

Smith, S. M., H. Johansen-Berg, M. Jenkinson, et al. 2007. "Acquisition and Voxelwise Analysis of Multi-Subject Diffusion Data With Tract-Based Spatial Statistics." *Nature Protocols* 2, no. 3: 499–503. https://doi.org/10.1038/nprot.2007.45.

Straka, B., B. Hermanovska, L. Krskova, et al. 2022. "Genetic Testing for Malformations of Cortical Development." *Neurology Genetics* 8, no. 5: e200032. https://doi.org/10.1212/NXG.0000000000200032.

Struck, A. F., C. Garcia-Ramos, and V. Prabhakaran. 2025. "Latent Cognitive Phenotypes in Juvenile Myoclonic Epilepsy: Clinical, Sociodemographic, and Neuroimaging Associations." *Epilepsia* 66, no. 1: 253–264. https://doi.org/10.1111/epi.18167.

Suzuki, T., A. V. Delgado-Escueta, K. Aguan, et al. 2004. "Mutations in EFHC1 Cause Juvenile Myoclonic Epilepsy." *Nature Genetics* 36, no. 8: 842–849. https://doi.org/10.1038/ng1393.

Tononi, G., and C. Cirelli. 2006. "Sleep Function and Synaptic Homeostasis." *Sleep Medicine Reviews* 10, no. 1: 49–62. https://doi.org/10.1016/j.smrv.2005.05.002.

Tononi, G., and C. Cirelli. 2014. "Sleep and the Price of Plasticity: From Synaptic and Cellular Homeostasis to Memory Consolidation and Integration." *Neuron* 81, no. 1: 12–34. https://doi.org/10.1016/j.neuron.2013.12.025.

Tournier, J. D., R. Smith, D. Raffelt, et al. 2019. "MRtrix3: A Fast, Flexible and Open Software Framework for Medical Image Processing and Visualisation." *NeuroImage* 202: 116137. https://doi.org/10.1016/j.neuroimage.2019.116137.

Tustison, N. J., B. B. Avants, P. A. Cook, et al. 2010. "N4ITK: Improved N3 Bias Correction." *IEEE Transactions on Medical Imaging* 29, no. 6: 1310–1320. https://doi.org/10.1109/TMI.2010.2046908.

Usui, N., P. Kotagal, R. Matsumoto, C. Kellinghaus, and H. O. Lüders. 2005. "Focal Semiologic and Electroencephalographic Features in Patients With Juvenile Myoclonic Epilepsy." *Epilepsia* 46, no. 10: 1668–1676. https://doi.org/10.1111/j.1528-1167.2005.00262.x.

Woermann, F. G., S. L. Free, M. J. Koepp, S. M. Sisodiya, and J. S. Duncan. 1999. "Abnormal Cerebral Structure in Juvenile Myoclonic Epilepsy Demonstrated With Voxel-Based Analysis of MRI." *Brain* 122, no. 11: 2101–2108. https://doi.org/10.1093/brain/122.11.2101.

Xu, N., W. Shan, J. Qi, J. Wu, and Q. Wang. 2021. "Presurgical Evaluation of Epilepsy Using Resting-State MEG Functional Connectivity." *Frontiers in Human Neuroscience* 15: 649074. https://doi.org/10.3389/fnhum.2021.649074.

Zhang, H., T. Schneider, C. A. Wheeler-Kingshott, and D. C. Alexander. 2012. "NODDI: Practical In Vivo Neurite Orientation Dispersion and Density Imaging of the Human Brain." *NeuroImage* 61, no. 4: 1000–1016. https://doi.org/10.1016/j.neuroimage.2012.03.072.

Supporting Information

Additional supporting information can be found online in the Supporting Information section.